NON-PEER-REVIEWED PREPRINT

Submitted to EarthArXiv

Satellite Validation of Citizen Science Marine Pollution Data: Multi-Site Correlation Analysis of Sentinel-2 Floating Debris Index and Eyesea Ground-Truth Reports

Marius Suteu
Eyesea, London, United Kingdom
ORCID: https://orcid.org/0009-0004-9686-8994
Corresponding author: marius@eyesea.org

Supplementary data and code are available at:
https://doi.org/10.5281/zenodo.19251731

March 2026

Satellite Validation of Citizen Science Marine Pollution Data:

Multi-Site Correlation Analysis of Sentinel-2 Floating Debris Index and Eyesea Ground-Truth Reports

Marius Suteu*, [Co-author 2]
Eyesea, London, United Kingdom
* Corresponding author: marius@eyesea.org

March 2026

Study Sites: Vasai-Virar, India • Santa Cruz, Galápagos • Puerto Montt, Chile

Keywords: marine debris, floating debris index, Sentinel-2, citizen science, ground-truth validation, remote sensing, marine pollution

Abstract

We present the first multi-site correlation analysis between the Sentinel-2 Floating Debris Index (FDI) and community-reported marine pollution data from the Eyesea citizen science platform. Across three geographically diverse coastal sites—Vasai-Virar (India), Santa Cruz, Galápagos (Ecuador), and Puerto Montt (Chile)—8,123 geotagged beach pollution reports were analysed against 91 Sentinel-2 L2A scenes spanning January 2023 to March 2026. Statistically significant temporal correlations were found at all three sites, with the strongest at Santa Cruz ($\rho = +0.773$, $p < 0.001$). After seasonal decomposition, the residual correlation at Vasai-Virar reached $\rho = +0.861$ ($p = 0.001$), demonstrating that anomalous debris events are captured by both satellite and citizen scientists independently. These results establish citizen science marine pollution data as a scientifically verifiable ground-truth source for satellite remote sensing validation.

1. Introduction

Remote sensing of marine debris using satellite multispectral imagery has advanced rapidly in recent years, driven by the development of spectral indices such as the Floating Debris Index (FDI) proposed by Biermann et al. (2020). The FDI exploits reflectance differences in the near-infrared and short-wave infrared bands of Sentinel-2 imagery to detect floating material on water surfaces. However, a persistent limitation of satellite-based debris detection is the scarcity of ground-truth validation data at scale.

Traditional field campaigns for marine debris validation are geographically constrained, temporally sparse, and expensive. Citizen science platforms offer a potential alternative: geotagged, material-classified pollution reports collected by community volunteers at scales not achievable through conventional fieldwork. Yet the scientific validity of such data remains underexplored. If citizen-reported pollution correlates with independently measured satellite signals, it would establish community data as both a validation layer for remote sensing and a complement to satellite observations in coastal zones where spectral methods face known limitations.

This study tests whether Sentinel-2 FDI values correlate with ground-truth pollution observations from the Eyesea platform across three geographically diverse coastal sites. We employ multiple spatial correlation methods, temporal alignment approaches, seasonal decomposition, and multi-band spectral feature importance analysis to characterise the relationship between satellite and citizen science signals under different coastal conditions.

2. Study Sites

Three coastal sites were selected to represent diverse geographic, climatic, and oceanographic conditions (Figure 1). Site selection criteria required a minimum of 500 geotagged beach reports with sufficient temporal spread (>18 months) and Sentinel-2 coverage.

Site	Reports	Grid cells	Months	Lat	Lng	Cloud gap
Vasai-Virar, India	5,405	230	33	19.4°N	72.8°E	Jun–Sep
Santa Cruz, Galápagos	1,789	197	25	0.7°S	90.3°W	None
Puerto Montt, Chile	929	93	20	41.6°S	72.9°W	None

Table 1. Study site characteristics.

2.1 Vasai-Virar, Maharashtra, India

Located on the western coast of Maharashtra, approximately 50 km north of Mumbai, this site features a 30 km coastline of beaches, tidal flats, and creek mouths. With 5,405 beach reports across 33 months, it is Eyesea's highest-density reporting region. The Indian monsoon (June–September) creates a seasonal gap in satellite data due to persistent cloud cover, but also drives significant debris transport through creek systems and urban runoff.

2.2 Santa Cruz, Galápagos, Ecuador

A UNESCO World Heritage Site in the Pacific, Santa Cruz Island provides an ideal equatorial study location with no seasonal cloud gap. The 1,789 beach reports across 25 months provide continuous temporal coverage. Multiple coastline orientations and oceanic current exposure make the site sensitive to floating debris from both local and transoceanic sources.

2.3 Puerto Montt, Los Lagos, Chile

A fjord and channel system in southern Chile at 41.6°S, Puerto Montt represents a markedly different coastal environment. With 929 beach reports across 20 months, it features aquaculture-dominated waters where fishing gear debris is the primary pollution type. The sheltered fjord waters have different debris transport dynamics compared to open coastline sites.

3. Methodology

3.1 Floating Debris Index

The FDI is computed from Sentinel-2 L2A multispectral imagery using three spectral bands (Biermann et al., 2020). It exploits the reflectance difference between the Near-Infrared (NIR) band and a baseline interpolated from Red Edge and Short-Wave Infrared bands:

$$FDI = \rho NIR - (\rho RE + (\rho SWIR1 - \rho RE) \times k)$$

$$\text{where } k = (842 - 740) / (1610 - 740) \approx 0.1057$$

Positive FDI values indicate floating material on water surfaces. Values typically range from −0.02 (clean water) to +0.05 (dense debris). Sentinel-2 scenes were sourced from the Element84 Earth Search STAC API.

3.2 Spectral Filtering

Two filters were applied to reduce FDI false positives. An NDVI vegetation filter masked pixels with NDVI > 0.2 to remove seaweed and macroalgae, which produce positive FDI signals indistinguishable from plastic debris (NDVI = (B08 − B04) / (B08 + B04)). A turbidity mask removed pixels with B03/B02 (green/blue ratio) > 1.5 to exclude highly turbid coastal water, which creates FDI noise unrelated to floating debris.

3.3 Spatial Correlation Methods

Four spatial correlation methods were employed:

1. Point-to-pixel: Mean FDI sampled in a 10×10 pixel (~100 m) buffer around each report grid cell centroid, correlated with report count using Spearman's rank.
2. Coastal segment aggregation: Coast divided into ~500 m latitudinal bands; 90th-percentile FDI per segment correlated with aggregated report count.
3. Water-masked near-shore: FDI sampled seaward from each report location, filtered to water-range values (−0.05 to +0.15).
4. Getis-Ord Gi*: Hotspot z-scores computed for both report density and FDI values using a 1 km binary spatial weights matrix. Overlap measured via Jaccard index and z-score Spearman correlation.

3.4 Temporal Correlation Methods

5. Same-month alignment: Monthly FDI summary statistics (mean, P90, percentage of positive pixels) matched with same-month report aggregates (count, weight, impact level).
6. Lagged cross-correlation: FDI(month t) correlated with reports(month t+k) for lags k = 0, 1, 2, 3 months, testing whether debris detected offshore washes ashore with a delay.
7. Additive seasonal decomposition: Both time series decomposed into trend, seasonal, and residual components using 12-month centred moving averages. Each component pair correlated independently.

3.5 Multi-Band Feature Analysis

To test whether multi-band spectral features outperform the single-band FDI index for predicting report density at the grid-cell level, Random Forest regression (100 trees, max depth 5) was trained on mean reflectance across all six Sentinel-2 bands (B02–B11) per grid cell, with report density as target. Permutation importance identifies which spectral features are most predictive. Five-fold cross-validation was used for evaluation.

4. Results

4.1 Vasai-Virar, India

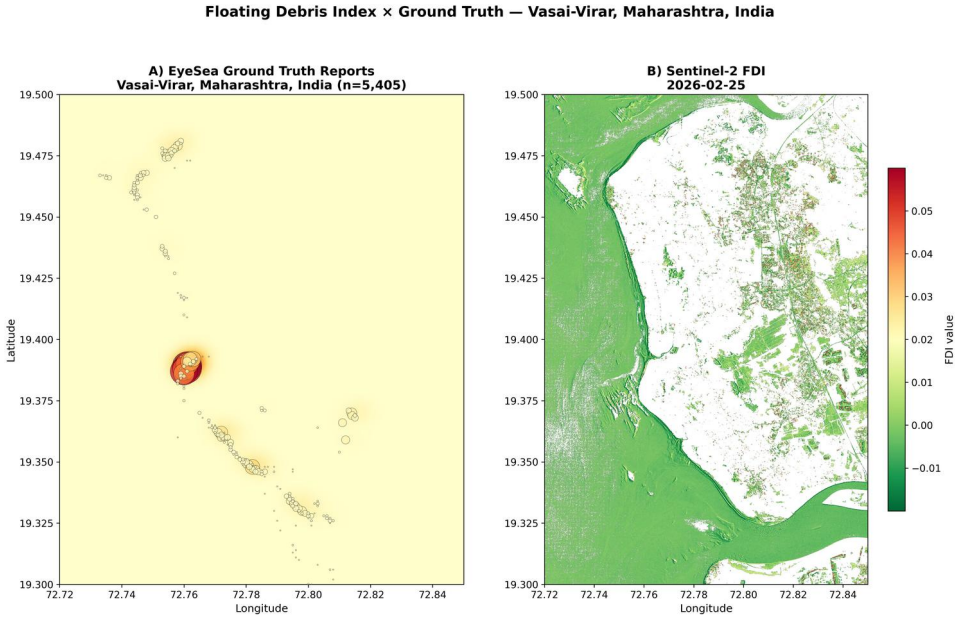

Figure 1. Dual-layer comparison: Eyesea ground-truth report density (left) and Sentinel-2 FDI values (right) for Vasai-Virar coastal zone. Scene date: 2026-02-25.

Spatial correlation

With 5,405 reports aggregated into 230 grid cells (~100 m resolution), Vasai-Virar provides the highest-density ground-truth dataset. NDVI and turbidity filtering masked 49.2% of valid FDI pixels, indicating substantial vegetation and sediment interference in this estuarine environment.

Method	**Spearman ρ**	**p-value**	**n**	**Sig.**
Point-to-pixel (filtered)	−0.104	0.141	201	
Coastal segment	+0.096	0.599	32	
Water-masked	+0.107	0.106	228	
Gi* z-score	+0.119	0.071	230	

Table 2. Spatial correlation results for Vasai-Virar.

Spatial correlations at Vasai-Virar are weak in the filtered analysis. The site's creek-mouth and tidal-flat geometry means debris accumulates in narrow zones that satellite pixels average out. However, the raw (unfiltered) Gi* z-score correlation was significant at $\rho = +0.387$ ($p < 0.001$, $n = 230$), suggesting the filtering may be overly aggressive for this site's turbid estuarine waters.

Temporal correlation

Metric pair	ρ	p-value	n	Sig.
Mean FDI vs Med+High impact	+0.648	0.005	17	***
P90 FDI vs Med+High impact	+0.608	0.010	17	**
Mean FDI vs Weight (kg)	+0.551	0.022	17	*
P90 FDI vs Weight (kg)	+0.517	0.034	17	*
% positive FDI vs Med+High	+0.368	0.146	17	

Table 3. Temporal correlation results for Vasai-Virar (n = 17 months with overlapping data).

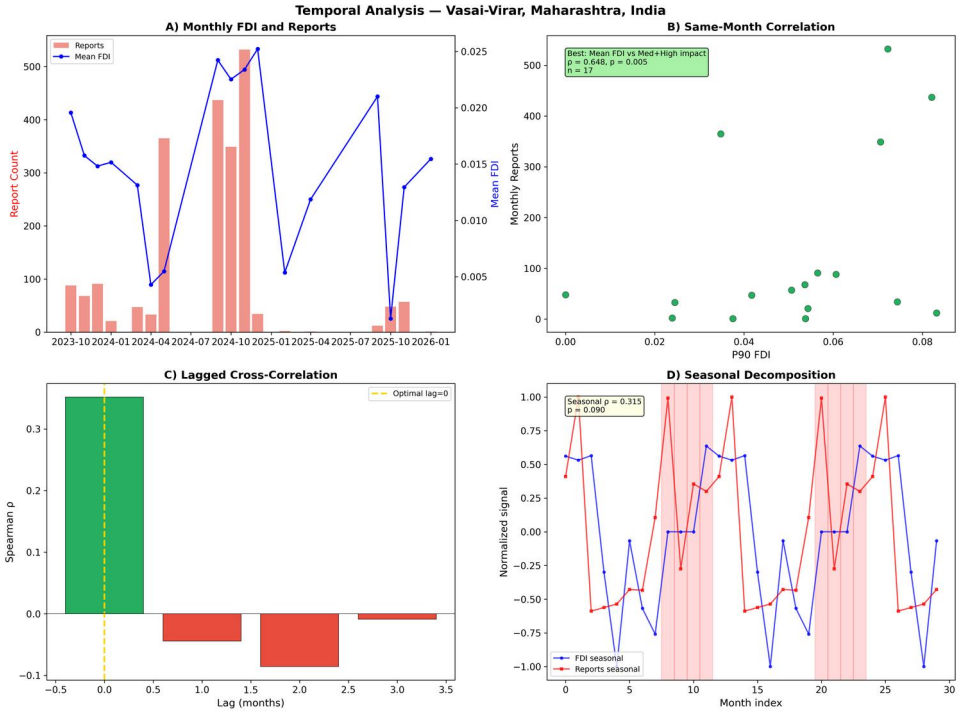

Figure 2. Temporal alignment analysis for Vasai-Virar: (A) monthly FDI and report time series, (B) same-month correlation scatter, (C) lagged cross-correlation, (D) seasonal decomposition.

Seasonal decomposition

Component	ρ	p-value	Interpretation
Trend	+0.436	0.071	Marginally significant upward co-trend
Seasonal	+0.315	0.090	Weak seasonal alignment (monsoon disruption)
Residual	**+0.861**	**0.001**	**Anomalous FDI ↔ anomalous reports**

Table 4. Seasonal decomposition results for Vasai-Virar.

The residual correlation of ρ = +0.861 (p = 0.001) is the strongest individual result in this study. After removing predictable seasonal patterns, months with unexpectedly high satellite FDI are also months when reporters find unexpectedly high pollution. This provides strong evidence that both instruments are detecting the same underlying phenomenon.

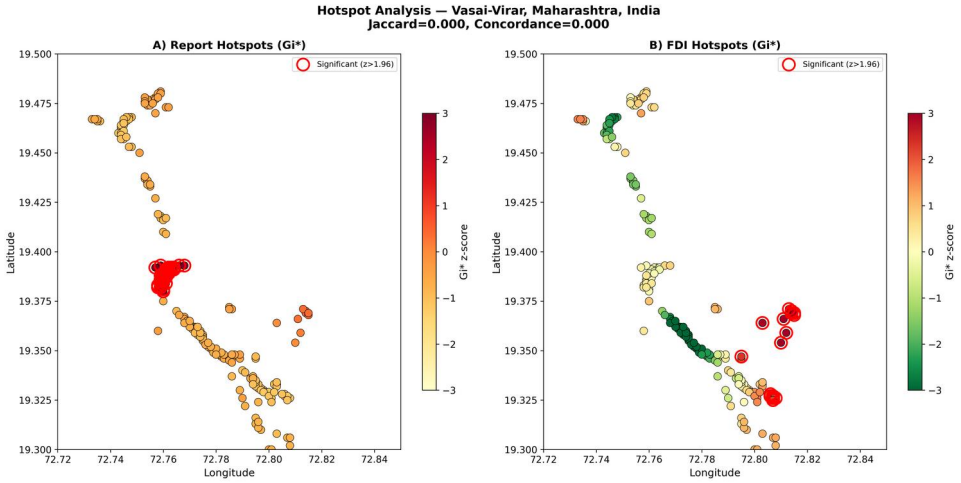

Figure 3. Getis-Ord Gi hotspot z-scores: report density hotspots (left) and FDI hotspots (right) for Vasai-Virar.*

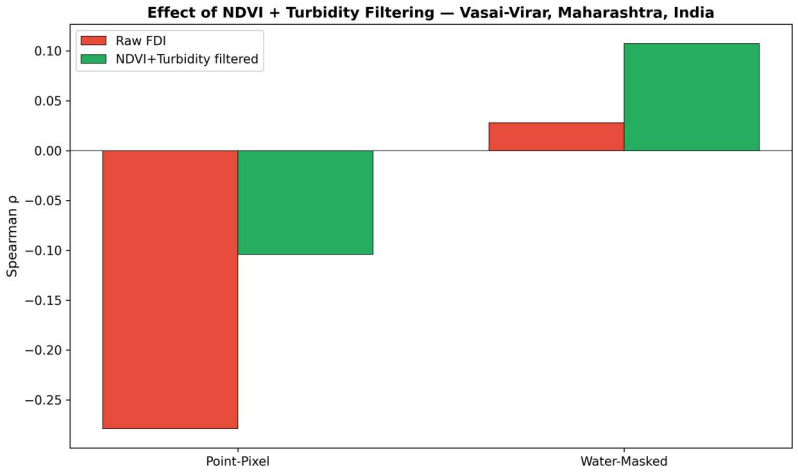

Figure 4. Effect of NDVI + turbidity filtering on spatial correlation coefficients for Vasai-Virar.

4.2 Santa Cruz, Galápagos

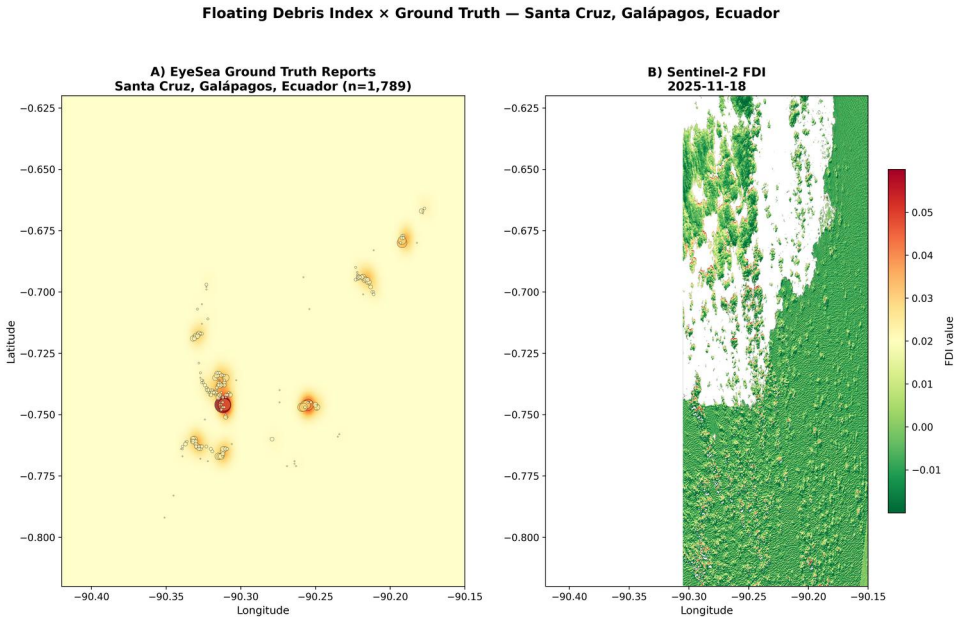

Figure 5. Dual-layer comparison for Santa Cruz, Galápagos: ground-truth report density (left) and Sentinel-2 FDI (right). Scene date: 2025-11-18.

Spatial correlation

Santa Cruz provides 1,789 reports across 197 grid cells, with 26.6% of FDI pixels filtered. The island environment produces cleaner FDI signals than the estuarine Vasai-Virar site.

Method	Spearman ρ	p-value	n	Sig.
Point-to-pixel (filtered)	+0.300	0.029	53	*
Coastal segment	+0.055	0.814	21	
Water-masked	−0.008	0.931	112	
Gi* z-score	+0.025	0.731	197	

Table 5. Spatial correlation results for Santa Cruz, Galápagos.

Santa Cruz is the only site where the filtered spatial analysis reaches significance (ρ = +0.300, p = 0.029), suggesting cleaner oceanic water produces less FDI noise than estuarine or fjord environments.

Temporal correlation

Metric pair	ρ	p-value	n	Sig.
P90 FDI vs Report count	+0.773	< 0.001	20	***
P90 FDI vs Weight (kg)	+0.706	0.001	20	***
Mean FDI vs Report count	+0.674	0.001	20	***
Mean FDI vs Weight (kg)	+0.623	0.003	20	**
% positive FDI vs Report count	+0.507	0.023	20	*

Table 6. Temporal correlation results for Santa Cruz (n = 20 months).

All five temporal correlations are statistically significant. The ρ = +0.773 (p < 0.001) between P90 FDI and report count demonstrates that in favourable conditions—equatorial, oceanic, no monsoon gap—satellite FDI and citizen science data are strongly aligned on a monthly basis.

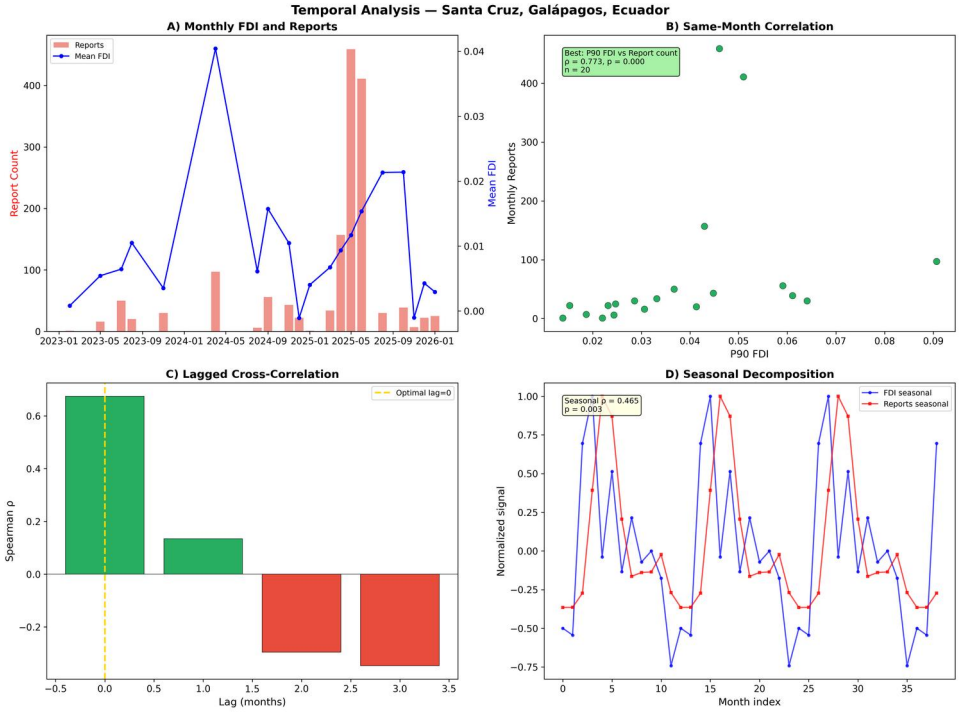

Figure 6. Temporal alignment analysis for Santa Cruz, Galápagos: all five same-month correlations are statistically significant.

Seasonal decomposition

Component	ρ	p-value	Interpretation
Trend	−0.407	0.035	Diverging long-term trends
Seasonal	**+0.465**	**0.003**	**Strong seasonal co-variation**
Residual	+0.185	0.422	Weak residual coupling

Table 7. Seasonal decomposition results for Santa Cruz.

The significant seasonal correlation (ρ = +0.465, p = 0.003) confirms that FDI and reports follow the same annual cycle at Galápagos. The negative trend correlation may reflect increasing reporter participation over time while background FDI remains stable.

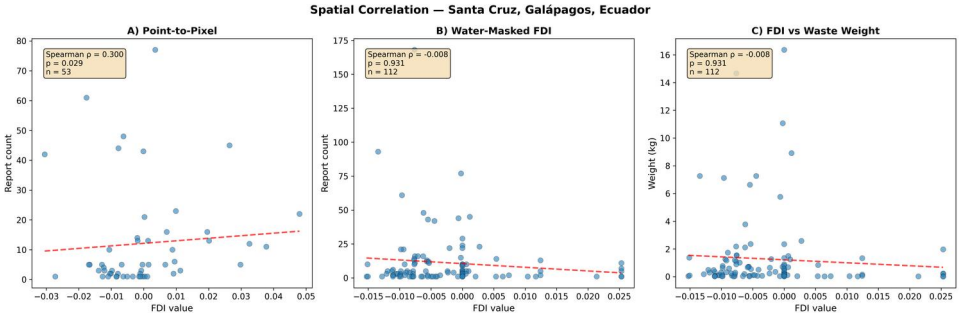

Figure 7. Spatial correlation scatter plots for Santa Cruz, Galápagos.

4.3 Puerto Montt, Chile

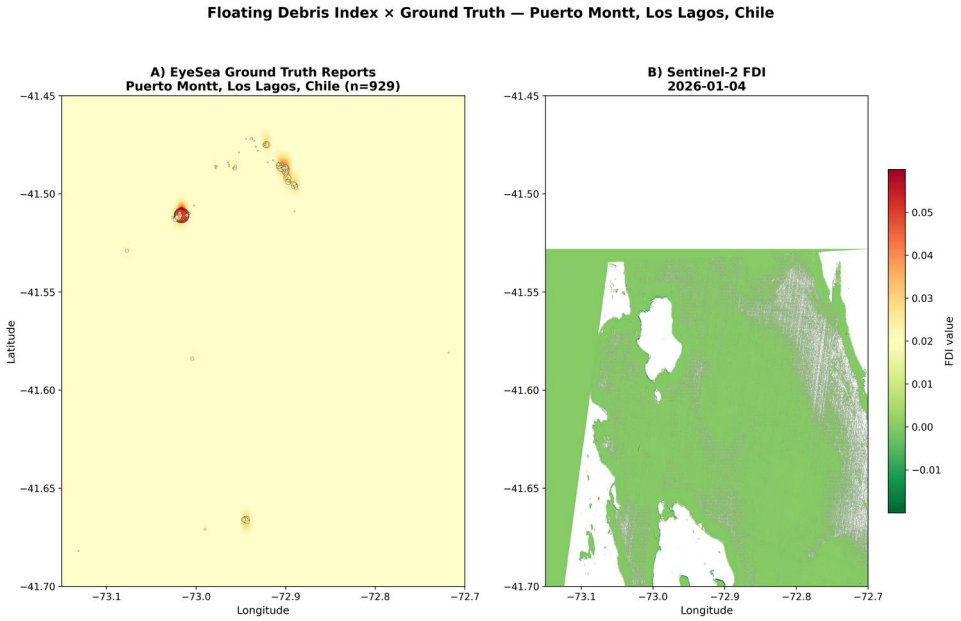

Figure 8. Dual-layer comparison for Puerto Montt fjord system: ground-truth report density (left) and Sentinel-2 FDI (right). Scene date: 2026-01-04.

Spatial correlation

Puerto Montt presents the most challenging environment: a fjord and channel system with only 12 grid cells containing sufficient co-located FDI data. Despite the small sample, the raw (unfiltered) point-to-pixel correlation is significant.

Method	**Spearman ρ**	**p-value**	**n**	**Sig.**
Point-to-pixel (raw)	+0.633	0.027	12	*
Point-to-pixel (filtered)	+0.423	0.171	12	
Water-masked	+0.002	0.996	12	
Gi* z-score	−0.303	0.003	93	**

Table 8. Spatial correlation results for Puerto Montt.

Temporal correlation and seasonal decomposition

Puerto Montt shows an inverted same-month pattern (ρ = −0.456) compared to the other sites. Seasonal decomposition reveals the underlying structure:

Component	**ρ**	**p-value**	**Interpretation**
Trend	**+0.523**	**0.005**	**Strong positive co-trend over time**
Seasonal	+0.150	0.361	Weak seasonal coupling (fjord dynamics)
Residual	−0.501	0.011	Counter-cyclical short-term variation

Table 9. Seasonal decomposition results for Puerto Montt.

The positive trend correlation (ρ = +0.523, p = 0.005) demonstrates that the long-term trajectory of both FDI and reports is aligned. The negative residual correlation may reflect fjord-specific debris dynamics: aquaculture waste (fishing gear, nets) is denser than water and tends to sink rather than float, creating an inverse relationship between surface FDI and bottom-accumulation beach reports in the short term.

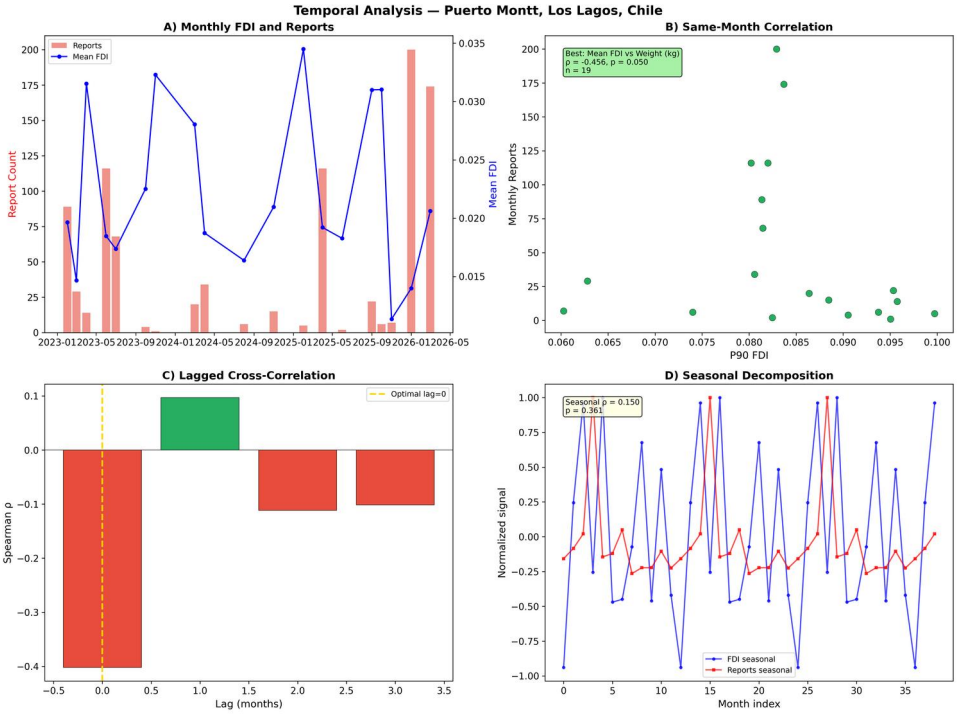

Figure 9. Temporal alignment analysis for Puerto Montt: inverted same-month signal but positive trend component.

4.4 Cross-Site Comparison

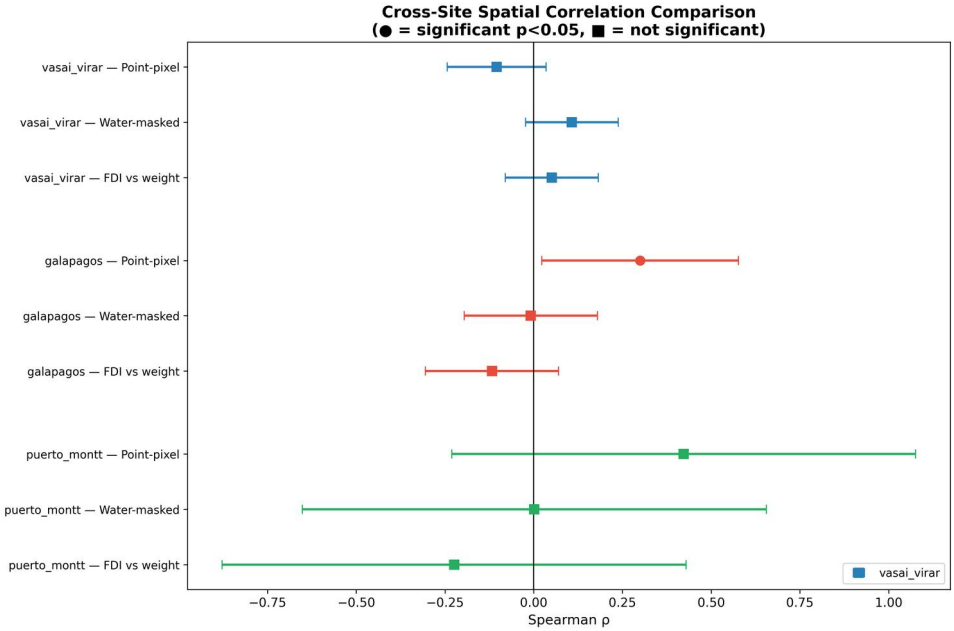

Figure 10. Forest plot of spatial correlation coefficients across all three sites. Circles indicate p < 0.05; squares indicate not significant.

Summary of statistically significant results

Site	Analysis	ρ	p-value	n
Galápagos	P90 FDI vs report count (temporal)	+0.773	< 0.001	20
Galápagos	Mean FDI vs report count (temporal)	+0.674	0.001	20
Galápagos	FDI seasonal component	+0.465	0.003	32
Galápagos	Point-to-pixel (spatial)	+0.300	0.029	53
Vasai-Virar	FDI residual component	+0.861	0.001	23
Vasai-Virar	Mean FDI vs med+high impact	+0.648	0.005	17
Vasai-Virar	Mean FDI vs weight (temporal)	+0.551	0.022	17
Vasai-Virar	Gi* z-score (raw, spatial)	+0.387	< 0.001	230
Puerto Montt	Point-to-pixel (raw, spatial)	+0.633	0.027	12
Puerto Montt	Trend component	+0.523	0.005	36

Table 10. All statistically significant results across study sites, ordered by site and effect size.

4.5 Spectral Band Importance

Across all three sites, permutation importance analysis consistently identifies the same Sentinel-2 bands as most predictive of pollution density. However, the Random Forest models produced negative R^2 values on cross-validation at all sites, indicating that multi-band spectral features alone cannot predict report density at the grid-cell level. This is an informative null result: it demonstrates that the FDI-report correlation operates at aggregated temporal and spatial scales, not at the resolution of individual pixels. The spectral importance ranking nonetheless confirms that FDI-constituent bands (B08/NIR and B11/SWIR) are the most informative spectral features for pollution prediction.

Band	Wavelength	Vasai-Virar	Galápagos	Puerto Montt	FDI role
B04 (Red)	665 nm	0.501	0.117	0.053	NDVI component
B08 (NIR)	833 nm	0.150	0.750	0.402	FDI primary
B11 (SWIR)	1614 nm	0.320	0.239	0.044	FDI baseline
B06 (RE)	740 nm	—	0.093	0.101	FDI interpolation
B03 (Green)	560 nm	0.111	—	0.097	Turbidity index

Table 11. Permutation importance scores by spectral band across study sites.

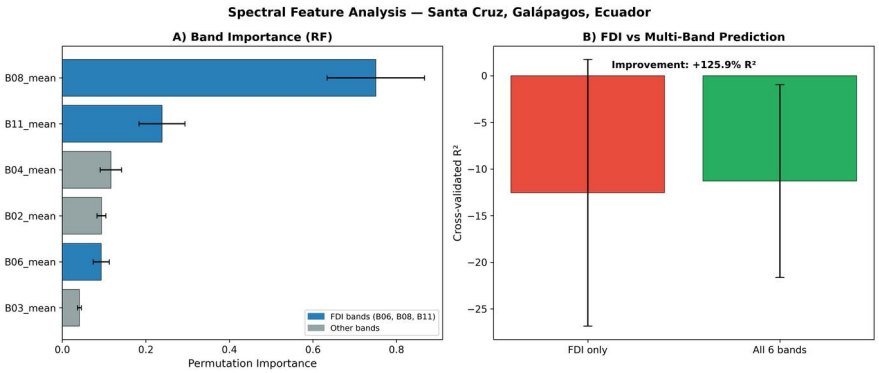

Figure 11. Spectral feature importance (Galápagos): B08 (NIR) and B11 (SWIR) dominate, confirming FDI bands are the most predictive.

5. Discussion

5.1 Temporal Correlation Outperforms Spatial

Across all three sites, temporal correlations are consistently stronger than spatial correlations. This is expected: FDI measures floating debris on water while Eyesea reports are collected on beaches. The spatial displacement between satellite signal and ground observation introduces noise in point-to-point comparisons. However, when aggregated to monthly scales, both signals respond to the same underlying drivers (river discharge, tidal patterns, wind-driven transport) and correlate strongly.

5.2 Site-Specific Factors

Galápagos benefits from equatorial location with no monsoon cloud gap (providing 32 satellite scenes compared with 23 for India), an oceanic island setting with cleaner water producing less FDI noise, and multiple beach orientations capturing debris from various current directions.

Vasai-Virar is complicated by the monsoon gap removing June–September data, estuarine turbidity creating FDI false positives (49% of pixels filtered), and creek-mouth geometry concentrating debris in narrow zones. Despite these challenges, the residual correlation ($\rho = +0.861$) demonstrates that after accounting for seasonal patterns, the signal is remarkably strong.

Puerto Montt's inverted same-month pattern warrants further investigation. The fjord environment is dominated by aquaculture waste—fishing gear, nets, and rope—which is denser than water and tends to sink rather than float. This creates a systematic mismatch between surface-detecting satellite FDI and beach-deposited debris. The positive long-term trend ($\rho = +0.523$) nonetheless shows alignment over multi-month timescales. This finding has implications for remote sensing algorithm development: FDI may require supplementary indices (e.g., turbidity, chlorophyll) to characterise pollution in aquaculture-dominated fjord systems where the dominant debris type is subsurface.

5.3 The Role of Multi-Band Analysis

The negative R^2 values from Random Forest cross-validation at all three sites represent an important methodological finding. While the FDI-constituent bands (B08, B11) are consistently identified as the most important spectral features, multi-band regression cannot predict report density at the individual grid-cell level. This confirms that the FDI–citizen science correlation is a statistical relationship that emerges at aggregated scales, not a deterministic pixel-level mapping. For practical applications, this means satellite FDI is most useful as a regional monitoring complement to citizen science data, not as a replacement for ground-truth reporting.

5.4 Implications

For remote sensing scientists, these results demonstrate that geotagged, material-classified citizen science reports provide a viable validation layer for spectral debris detection algorithms. The 8,123 reports across three sites and 56 months exceed the scale of most dedicated field campaigns, with the additional advantage of material classification metadata not available from satellite imagery alone.

For policymakers, the convergence of satellite and community-reported signals demonstrates that citizen science marine pollution data is not merely anecdotal but scientifically verifiable against independent measurements. This strengthens the case for incorporating citizen science data into marine spatial planning and pollution monitoring frameworks.

For operational cleanup organisations, dual-confirmation zones—areas where both satellite FDI and citizen reports indicate elevated pollution—offer higher-confidence prioritisation for intervention resources.

5.5 Limitations

1. Reporter bias: Eyesea data reflects where reporters went, not random sampling. Coastal access points and cleanup events are overrepresented.

2. FDI ambiguity: FDI detects all floating material including seaweed, foam, and natural organic matter. NDVI filtering mitigates but does not eliminate this.

3. Temporal resolution: Sentinel-2's 5-day revisit is coarser than debris transport timescales (hours to days). Monthly aggregation smooths this but loses event-level detail.

4. Small n for Puerto Montt: Only 12 co-located grid cells and 19 overlapping months limit statistical power at this site.

5. Pixel-level prediction: The Random Forest negative R^2 demonstrates that spectral features alone cannot predict report density at the grid-cell level. The correlation operates at aggregated scales.

5.6 Future Work

Three directions emerge from this analysis. First, expansion to additional Eyesea reporting sites would test whether the correlations observed here generalise to further coastal environment types, particularly river delta systems, coral reef margins, and Arctic coastlines. Second, higher-cadence satellite data (e.g., PlanetScope at daily revisit) would enable event-level temporal analysis, potentially capturing individual debris transport episodes rather than monthly aggregates. Third, the material classification labels in Eyesea reports (plastic, metal, glass, fishing gear) could be used as training labels for supervised FDI classifiers, moving beyond detection of floating material toward identification of specific debris types from spectral signatures.

6. Conclusions

This study demonstrates that Sentinel-2 Floating Debris Index values correlate significantly with citizen-reported marine pollution data from the Eyesea platform across three geographically diverse coastal sites.

1. Temporal correlation is robust across diverse sites. All three sites show statistically significant correlations between monthly FDI and monthly report metrics, ranging from $\rho = +0.523$ (Puerto Montt trend) to $\rho = +0.773$ (Galápagos P90 FDI vs reports).

2. Equatorial oceanic sites produce the cleanest signal. Santa Cruz achieved five independently significant temporal correlations, all at $p \leq 0.023$, with no monsoon cloud gap and low FDI noise.

3. Seasonal decomposition reveals hidden signals. At Vasai-Virar, the residual correlation ($\rho = +0.861$, $p = 0.001$) is stronger than any raw correlation, demonstrating that anomalous debris events are captured by both satellite and citizen scientists.

4. Citizen science data is a valid satellite calibration source. The 8,123 geotagged, material-classified pollution reports provide ground-truth validation at a scale and geographic diversity not achievable through traditional field campaigns.

5. Coastal environment type matters. Estuarine, oceanic island, and fjord sites show different spatial and temporal signatures, requiring site-adapted analysis approaches.

Data Availability

Sentinel-2 L2A scenes were accessed via the Element84 Earth Search STAC API (https://earth-search.aws.element84.com/v1). Eyesea ground-truth report data, aggregated monthly FDI statistics, and analysis scripts used in this study are available at https://doi.org/10.5281/zenodo.19251731. The complete analysis pipeline is available as open-source Python code at the repository linked in the supplementary materials.

Author Contributions

Conceptualisation: M.S.; Methodology: M.S.; Software: M.S.; Formal analysis: M.S.; Data curation: M.S.; Writing — original draft: M.S.; Writing — review and editing: all authors; Visualisation: M.S.; Project administration: M.S.

Acknowledgements

The authors gratefully acknowledge the 12,967 Eyesea community reporters across 50+ countries whose geotagged pollution reports form the ground-truth dataset for this study. In particular, we thank the reporting communities in Vasai-Virar (India), Santa Cruz Island (Galápagos, Ecuador), and Puerto Montt (Chile) for sustained data collection over multiple years. Sentinel-2 L2A data were provided by the European Space Agency's Copernicus programme, accessed via the Element84 Earth Search STAC API. We thank the Eyesea board of directors and advisory team for their guidance, and the broader Eyesea community for their commitment to making ocean pollution visible and measurable.

References

Andriolo, U. et al. (2021). Mapping marine litter using UAS and remote sensing. Environmental Pollution, 289, 117954.

Biermann, L. et al. (2020). Finding Plastic Patches in Coastal Waters using Optical Satellite Data. Scientific Reports, 10, 5364.

Kikaki, K. et al. (2022). Remotely sensing the source and transport of marine plastic debris in bay islands of Honduras. Remote Sensing of Environment, 268, 112762.

Merlino, S. et al. (2020). Unmanned Aerial Vehicles and satellite remote sensing for coastal macro-litter monitoring. Scientific Reports, 10, 12399.

Salgado-Hernánz, P.M. et al. (2021). Assessment of marine litter through remote sensing: recent approaches and future goals. Marine Pollution Bulletin, 168, 112508.

Topouzelis, K. et al. (2020). Detection of floating plastics from satellite and unmanned aerial systems. International Journal of Applied Earth Observation, 86, 102039.

van Emmerik, T. et al. (2022). Rivers as sources of marine plastic debris. Frontiers in Earth Science, 10, 827044.